Large Eddy Simulation of the flow past a square cylinder

J.S. Ochoa *,   N. Fueyo

Área de Mecánica de Fluidos, Centro Politécnico Superior, C/Maria de Luna 3 50018 Zaragoza, Spain

---

Abstract

Turbulence is a phenomenon that occurs frequently in nature and that is also a situation present in almost all industrial applications. In this work, the simulation of turbulent vortex shedding from a bluff-body square cylinder has been undertaken using Large Eddy Simulation technique (LES). The objective of this work was to implement this type of simulations in parallel PHOENICS and validate the results in order to apply them to practical cases like bluff-body jet burners. The LES Smagorinsky model and auxiliary calculations like Adam-Moulton high order time scheme have been implemented as FORTRAN subroutines into the code. The turbulent flow has a Reynolds number of 21400 and it corresponds to a flow of water over a square cylinder. This has been previously used by several authors to validate turbulence CFD models. The influences of the LES model and numerical schemes are analyzed and the most important flow parameters are calculated. The results agree with experimental and numerical available data. Also, a comparison between using LES and Reynolds Averaged Navier-Stokes Equations with the $k - \epsilon$ model have been made and some differences are pointed out. The results allow to conclude that the LES model improves the accuracy of the the $k - \epsilon$ model and reproduces adequately the flow motion and the vortex shedding. The simulation has been performed in parallel mode on a varying number of nodes of a 66-processor cluster. The parallel calculation results in significant time savings compared with the sequential (single-processor) run. The next step will be to apply this model to a bluff-body flame in order to study the interaction between turbulence and chemistry in industrial burners.

Keywords: Turbulence, Large Eddy Simulation, LES, vortex shedding, square cylinder

---

Nomenclature

k	turbulent kinetic energy $[\frac{m^2}{s^2}]$
ϵ	dissipation rate of k $[\frac{m^2}{s^3}]$
H	length of the side of the square cylinder $[m]$

---

* Corresponding author. Tel. +34 976 761 000 ext. 5052
  Email address: sochoa@mafalda.cps.unizar.es (J.S. Ochoa).

Nomenclature cont.

U	reference velocity $[\frac{m}{s}]$
f	shedding frequency $[Hz]$
St	Strouhal number
Re	Reynolds number
ν	kinematic viscosity $[\frac{m^2}{s^2}]$
Cw	channel width $[m]$
Ch	channel height $[m]$
ρ	density $[\frac{kg}{m^3}]$
t	time $[s]$
$\vec{u}$	velocity $[\frac{m}{s}]$
p	pressure $[\frac{N}{m^2}]$
$\vec{\vec{\tau}}$	viscous stresses $[\frac{N}{m^2}]$
$\underline{f_m}$	body forces $[\frac{N}{m^3}]$
$\overline{g(x)}$	(any) filtered function
Δ	filter's length scale $[m]$
μ	dynamic viscosity $[\frac{kg}{ms}]$
τ_{ij}^s	subgrid scale (SGS) Reynolds stress $[\frac{N}{m^2}]$
ν_T	eddy viscosity $[\frac{m^2}{s^2}]$
$\overline{S}_{ij}$	filtered strain rate $[s^{-1}]$
$|\overline{S}|$	turbulence-energy-generation rate $[s^{-2}]$
C_s	Smagorinsky constant
ϕ	a generic transported variable [ϕ's units]
$f(\phi,t)$	all the terms of a transported equation, except the temporal term $[\frac{\phi_{units}}{m^3}]$
Δt^{CFL}	Courant condition's time step $[s]$
u, v, w	velocity components $[\frac{m}{s}]$
C_D, C_L	mean drag and lift coefficients
T	Vortex shedding period $[s]$
C_μ	$k - \epsilon$ model's constant
S_n	speedup factor

1 Introduction

Turbulence is a phenomenon that occurs frequently in fluid flow, both in Nature and in almost all industrial flows. This fact strongly motivates researchers to study this type of flows. The wide spatial and temporal scale ranges of turbulent flows make the Direct Numerical Simulation, or DNS, impractical nowadays except for a small Reynolds number. Customarily, models that solve the Reynolds-Averaged Navier-Stokes (RANS) equations are used for simulations of practical interest, but these have many fundamental limitations; from the standpoint of the present paper, one of such limitations is their inability to predict both the periodic and

Table 1
Main parameters of Lyn and Rodi's experiment ([3] [4])

Parameter	value
Square cylinder side	$H = 0.04$ m
Inlet velocity	$U = 0.535$ m/s
Reynolds number	$Re = UH/\nu = 21400$
Channel width	$Cw = 0.40$ m
Channel height	$Ch = 0.56$ m
Strouhal number	St $= 0.132$

the turbulent nature of some flows. Large Eddy Simulation (LES) is an intermediate alternative between DNS and RANS that provides three dimensional time dependent solutions of Navier-Stokes Equations. Although it still requires considerable computational resources, LES is being increasingly used in practical applications due to the unrelenting advances in computer processors. In this work, LES is implemented into PHOENICS, together with improved numerical and spatial resolution schemes. The algorithm is applied to the simulation of the vortex shedding from a square cylinder, which is an experimentally well-documented case. In this paper 2D and 3D simulations are presented, together with a parametric evaluation of the LES model and the implemented schemes. The 3D results are validated against available experimental data, as well as against the results from other numerical simulations. A comparison between $k - \epsilon$ RANS models and LES is carried out and differences are stated. Simulations are performed in parallel on a Beowulf-type machine.

2 The problem considered

The flow concerned in this study corresponds to a turbulent flow of water around a square cylinder, as studied experimentally by Lyn and Rody [3] and Lyn *et al.* [4]. The side of the square cylinder (H) is 0.04m and it extends along the width of the channel, the cross-section of which is 0.40x0.56m. All distances are made non-dimensional with reference to H. The mean velocity at the inlet, U, is assumed to be 0.535m/s and it is taken as a reference value. All velocities are made non-dimensional with this value. The Reynolds number, based on U and H, is 21400. The shedding frequency, f, is estimated experimentally to be 1.77Hz. The resulting Strouhal number ($St = fH/U$) is 0.132. A summary of the main flow parameters is shown in table 1. Since the flow involves coherent shedding of vortices from the cylinder, it becomes an interesting flow to use as a test case for LES. In fact, it has been selected by many authors as a test case to validate turbulence models [23],[27], [2]. It has also featured as a test case in some workshops about LES [28], [29]. Further details and results about the flow and these workshops can be found in the ERCOFTAC web site.[32].

3 Modelling

3.1 Equations

The equations describing the dynamics of the flow are the equations of continuity and momentum. These are (for an incompresible flow):

$$\nabla \cdot (\rho \vec{v}) = 0 \qquad (1)$$

3

$$\frac{\partial(\rho\vec{v})}{\partial t} + \nabla \cdot (\rho\vec{v}\vec{v}) = -\nabla p + \nabla \cdot \vec{\vec{\tau'}} + \rho\vec{f}_m \tag{2}$$

where $\vec{\vec{\tau'}}$ is the viscous stress tensor and f_m stands for the body forces.

3.2 Filtered equations

The objective of Large Eddy Simulations is to explicitly simulate the large scales of a turbulent flow while modelling the small scales. This is best done by filtering the equations [1]. Using one dimensional notation for convenience (generalization to the three-dimensional case is straight-forward), the filtered velocity is defined by:

$$\bar{u}_i = \int G(x, x')u_i(x')dx' \tag{3}$$

where $G(x, x')$, the filter kernel, is a localized function which can have several shapes (for instance, a Gaussian filter, a box filter or a cutoff filter) [9]. Every filter can be associated with a length scale, Δ. Thus, in a general sense, eddies of size larger than Δ are large eddies and correspond to the resolved scales, while those smaller than Δ are the small eddies that will need to be modelled. When filtering is applied to the Navier-Stokes equations (for incompressible flows), a set of equations similar to the RANS ones is obtained:

$$\frac{\partial \bar{u}_i}{\partial x_i} = 0 \tag{4}$$

$$\frac{\partial(\rho\bar{u}_i)}{\partial t} + \frac{\partial(\rho\overline{u_i u_j})}{\partial x_j} = -\frac{\partial \bar{p}}{\partial x_i} + \frac{\partial}{\partial x_j}[\mu(\frac{\partial \bar{u}_i}{\partial x_j} + \frac{\partial \bar{u}_j}{\partial x_i})] \tag{5}$$

From equation 5, it can be observed that the non-linearity of the momentum equation produces an analog term to the Reynolds stress of RANS. As in RANS, one has:

$$\overline{u_i u_j} \neq \bar{u}_i \bar{u}_j \tag{6}$$

and the quantity on the left-hand side of the inequality cannot be computed. The balance in this inequality results in the term:

$$\tau_{ij}^s = \overline{u_i u_j} - \bar{u}_i \bar{u}_j \tag{7}$$

where τ_{ij}^s is the subgrid scale (SGS) Reynolds stress, which must be modelled. This is not physically a stress, but rather the large scale momentum flux caused by the action of the small or unresolved scales. Further references on LES are [7], [8], [13], [14], [24]. Upon substituting equation 7 into 5, the next equation is obtained:

$$\frac{\partial(\rho\bar{u}_i)}{\partial t} + \frac{\partial(\rho\bar{u}_i\bar{u}_j)}{\partial x_j} = -\frac{\partial \bar{p}}{\partial x_i} + \frac{\partial}{\partial x_j}[\mu(\frac{\partial \bar{u}_i}{\partial x_j} + \frac{\partial \bar{u}_j}{\partial x_i}) + \tau_{ij}^s] \tag{8}$$

The approximation of τ_{ij}^s in equation (8) is the main topic of LES, and it originates the different types of LES models. In this paper, the Smagorinsky model has been used. This is described in the next section.

3.3 Smagorinsky Closure

This model was proposed by Smagorinsky in 1963 [11] and it is nowadays one of the most-commonly employed. Some authors consider this model as the LES version of the well-known mixing-length model of Prandtl [29]. Making an analogy with the effects of stress in laminar flows, the SGS can be written as:

$$\tau_{ij}^s - \frac{1}{3}\tau_{kk}^s \delta_{ij} = -2\nu_T \overline{S}_{ij} \tag{9}$$

where ν_T is the eddy viscosity, while $\overline{S}_{ij}$ refers to the strain rate in the resolved velocity field, which is in turn defined by:

$$\overline{S}_{ij} = \frac{1}{2}\left(\frac{\partial \overline{u}_i}{\partial x_j} + \frac{\partial \overline{u}_j}{\partial x_i}\right) \tag{10}$$

Using dimensional analysis, it can be proven that a reasonable form of the eddy viscosity is:

$$\nu_T = (C_s \Delta)^2 |\overline{S}| \tag{11}$$

where $|\overline{S}| = (2\overline{S}_{ij}\overline{S}_{ij})^{\frac{1}{2}}$; Δ is the length associated with the filter, this length is defined as: $\Delta = (\Delta_x \Delta_y \Delta_z)^{\frac{1}{3}}$. The term C_s is a parameter that can be assigned from different theories which suggest that for isotropic turbulence, for instance, $C_s \approx 0.2$. However, this parameter can be a function of other parameters such as the Reynolds number. For example, it has been found that, to simulate a channel flow, C_s has to be reduced from 0.2 to 0.065 which results in the reduction of the eddy viscosity by almost an order of magnitude [8]. Additionally, in regions close to walls, the value has to be reduced even further. An approach that has been used successfully is the van Driest damping that is commonly used to reduce the near-wall eddy viscosity in RANS models. This damping function acts on the C_s parameter as:

$$C_s = C_{s0}\left(1 - e^{\frac{-y^+}{A^+}}\right)^2 \tag{12}$$

where y^+ is the distance from the wall in viscous wall units ($y^+ = yu_\tau/\nu$) and A^+ is a constant usually considered to be approximately 25. The value of C_{s0} was taken as 0.1 which is commonly used in literature for turbulence with gradients of mean velocity.

3.4 Domain, grid and boundary conditions

The computation has been carried out in a domain corresponding to that used for the Workshop on LES organized by Rodi and Ferziger [28], and in the second conference of ERCOFTAC on DNS and where the problem featured LES as a test case [29], [32]. The domain is shown in figure 1.

In this paper, 2D and 3D simulations are performed. The three-dimensionality of turbulence cannot be questioned. It has been stated in the past ([26], [30]) that 2D LES calculations are clearly inferior to the three-dimensional ones since certain important features of turbulence
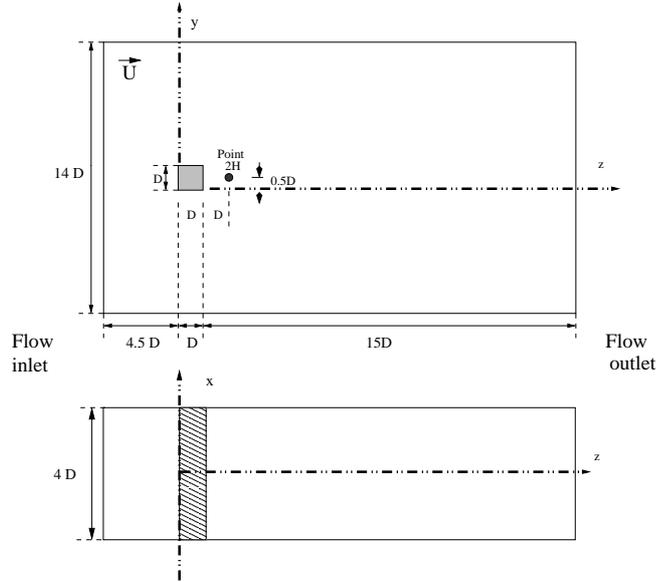
Fig. 1. The geometry of the square cylinder flow

are not resolved, for example, the vortex formation in the spanwise direction. However, some authors [2] have concluded that by means of a denser 2D grid the quasi-two-dimensional mechanism can be accurately evaluated, mainly at the regions closest to the solid walls. This practice allows an obvious saving in computation time. The aim of the two-dimensional simulations in this work is to evaluate by means of economical simulations the LES model, the implemented schemes and the grid influences. Therefore, several levels of mesh size are used in this type of simulations. The 3D grid and the domain can be seen in figure 2. The mesh is not uniform (being denser near the square cylinder), and the number of nodes is 120x102x20. At the inflow plane constant velocity is imposed (no perturbations added). A convective boundary condition is utilized at the outflow boundary. Logarithmic wall-functions are applied on the cylinder walls and at lateral walls free-slip conditions are used.

3.5   *Convective and temporal discretization*

A second-order Van Leer scheme is selected for simulating the convective transport in the momentum equations [31].

For the discretization in time, a third-order-implicit Adam-Moulton scheme is implemented. According to this scheme, the value in each node of a variable ϕ can be calculated as:

$$\phi^n = \phi^{n-1} + \frac{\Delta t}{12}[5f(t_n, \phi^n) + 8f(t_{n-1}, \phi^{n-1}) - f(t_{n-2}, \phi^{n-2})] \tag{13}$$

where n stands for the current time step, $(n-1)$ and $(n-2)$ are previous steps. The function $f(t, \phi)$ stands for all terms of the transport equations except the temporal term. The value of time step dt according to the Courant condition is calculated as:

$$\Delta t^{CFL} = min[(\frac{\Delta x}{u}), (\frac{\Delta y}{v}), (\frac{\Delta z}{w})] \tag{14}$$
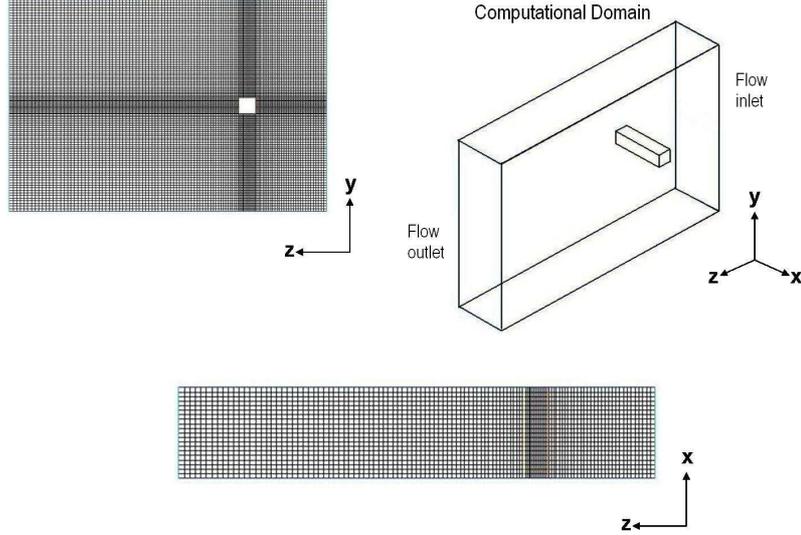
6

Fig. 2. Cartesian computacional grid (120x102x20) used in the present study for LES of turbulent flow past a square cylinder

The purpose of this calculation is to capture all time scales from the cell residence time. The value taken is the minimum for the whole domain. The flow was simulated over 3600 time steps, which are equivalent to roughly seven times the residence time.

3.6 Other auxiliary parameters

An extra transport equation has been set up to solve for a passive scalar called the mixture fraction f. This scalar is assigned the value of one over one half of the inlet, and zero over the other half, and it used to better visualize the vortical structures. The Strouhal Number is a non-dimensional vortex-shedding frequency, and is calculated as:

$$St = \frac{fH}{U} \tag{15}$$

where f is the vortex shedding frequency, H is the square-cylinder side and U is the reference velocity assumed at the inlet of the domain.

The mean drag and lift coefficients, C_D and C_L have also been calculated, as have their rms values, C_D^{rms} and C_L^{rms}. These coefficients are given by the following expressions:

$$C_D = \frac{F_{horizontal}}{\frac{1}{2}\rho U^2} \tag{16}$$

$$C_L = \frac{F_{vertical}}{\frac{1}{2}\rho U^2} \tag{17}$$

where U is the reference velocity. Forces, F, can be calculated on each side of the cylinder as:

$$\vec{F} = \int_s \vec{n} \cdot \vec{\vec{\tau}} ds \qquad (18)$$

where $\vec{\vec{\tau}}$ is the stress tensor.

All these parameters are calculated by averaging over the last 12 vortex shedding cycles of the simulation (and once a steady shedding is obtained).

3.7 Implementation in PHOENICS

The simulations have been carried out using parallel PHOENICS, version 3.5. The simulation features and models have been defined by means of the PIL (*PHOENICS Input Language*) and GROUNG facilities. Several GROUND subroutines are used to implement the LES model, and to calculate several special sources and all the auxiliary parameters during the simulation. The main settings of the simulation are summarized in the next sections, loosely following the same group structure of PHOENICS.

- *Time and spatial discretisation*
  The flag $STEADY=F$ enables the transient formulation of PHOENICS. The timestep-size is optionally controlled by setting $TLAST=GRND$. The Courant-limited explicit time-step is computed in a GROUND module, and this can be used as reference for both implicit and explicit calculations. The limiting timestep for the next step is calculated at the end of the previous one on every subdomain using the convection fluxes as follows:

$$DT_{explicit} = \frac{MASS1}{max(CON1E, CON1N, CON1H)} \qquad (19)$$

.

  By using MPI commands the limiting timestep computed locally is broadcast to all processors in order to get the overall limit for the whole domain. The resulting value is thereafter used in the next timestep.

  The high-order, implict Adam-Moulton discretisation in time is implemented by computing and adding special sources from a GROUND subroutine. This scheme is summarised below. Let the term $f(t_n, \phi^n)$ stand for all the terms in a transport equation, except the temporal term, at time level n. After the second timestep, it is possible to compute the term $f(t_n, \phi^n)$ as:

$$\frac{\phi^n - \phi^{n-1}}{\Delta t} = f(t_n, \phi^n) \qquad (20)$$

.

  The value of the function f is stored in temporary $GXMAKE$ arrays RHS_n for several time-levels n. (For the current timestep, RHS_n is not in fact available in exact form until the end of sweeping; but it is estimated at half the number of sweeps.) The Adam-Moulton

scheme is applied from the fourth time step by adding to the equation source term (in the corresponding Group 13 of GROUND), calculated from the value of the stored values of $f(t_n, \phi^n)$ at three time levels as:

$$\underbrace{\frac{\phi^n - \phi^{n-1}}{\Delta t} = f(t_n, \phi^n)}_{Common\ formulation\ of\ PHOENICS} \quad \underbrace{-\frac{7}{12}[RHS_n] + \frac{2}{3}[RHS_{n-1}] - \frac{1}{12}[RHS_{n-2}]}_{Special\ sources\ added} \quad (21)$$

.

An explict, second-order-accurate Adam-Bashford scheme is implemented using similar principles.

The setting $CARTES=T$ is used to select a Cartesian coordinate system. The size of the spatial domain and the grid features have also been defined by means of $GRDPWR$. A power-law exponent is used to increase the grid resolution close to the square cylinder. The high-order $VANL1$ scheme is applied to the momentum equations by means of the command $SCHEME$.

- *Variables solved and stored and flow properties*
  A set of five variables are solved for($P1$, $U1$, $V1$, $W1$ and $MIXF$). The whole-field option is activated for all of them. Storage has been provided for thermodynamic and transient properties such as density ($RHO1$), and laminar and turbulent viscosities ($ENUL$ and $ENUT$). Other variables are used to store auxiliary fields such as convection fluxes across the cell faces (i.e. the mass flow rates $CON1E$, $CON1N$ and $CON1H$). By setting $GENK=T$ and $YPLS=T$, the storage of the velocity gradients and some turbulent quantities such as the turbulent generation function ($GEN1$) and the non-dimensional wall distance ($YPLS$) is activated.

- *Turbulence model*
  The Smagorinsky model is activated by setting $ENUT=GRND$ and not by using the $TURMOD$ command of PHOENICS. During the simulation, group 9 section 5 of a special GROUND subroutine is visited. In this ground module, temporary variables and arrays (made by means of $MAKE$ and $GXMAKE$) are allocated and the necessary calculations for this eddy-viscosity model are effected. The viscosity is calculated in this GROUND section are calculated as:

$$VIST = (C_S * DELTA_{filter})^2 * SQRT(GEN1) \quad (22)$$

$$C_S = C_{S0} * (1 - EXP(-YPLS/A)) \quad (23)$$

$$DELTA_{filter} = (DX * DY * DZ)^{\frac{1}{3}} \quad (24)$$

where C_{S0} and A are constants that are transmitted to GROUND using the RG array of PIL.

When the $k - \epsilon$ model is used, the PHOENICS implementation ($KEMODL$) is used.

- *Special sources and initial and boundary conditions*

9

Trivial initial conditions are normally used. The simulation is left to evolve several times the oscillation period, T, so that the initial conditions do not have any influence on the simulation. This requires approximately 3600 timesteps.

In group 13 of the Q1 file, the inlets and outlets are defined by means of *PATCH* and *COVAL* commands. The special sources of the Adam-Moulton scheme are defined in this group with a *PATCH* involving the whole domain and *GRND* as *VALUE* argument of *COVAL* for all the solved-for variables except *P1*. Group 13 section 12 of GROUND is visited in order to add the special sources, according to equation 21
. *WALL* commands are used to define the logarithmic wall-functions around the square cylinder.

A GROUND subroutine dumps and stores data such as simulation time and fluid velocities for post-processing. Other GROUND subroutines are implemented to compute the drag and lift coefficients and the vorticity field. All the necessary parameters and constants (such as the Smagorinsky constant, the positions selected to dump data and the switches used to select the GROUND-implemented schemes) are specified by using the PIL arrays *LG*, *RG* and *IG*.

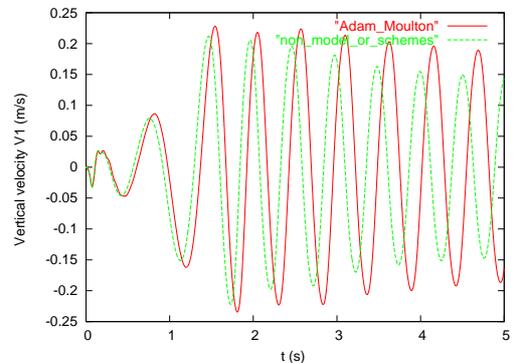Fig. 3. Effect of the Van Leer scheme

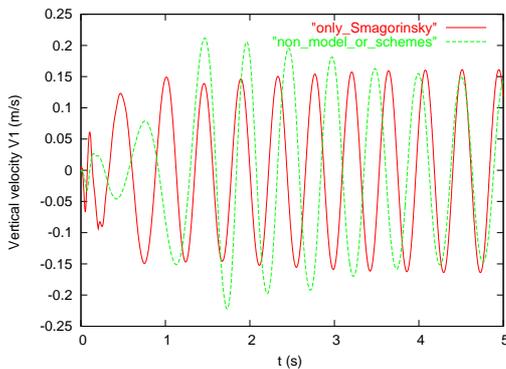Fig. 4. Effect of the Adam-Moulton scheme
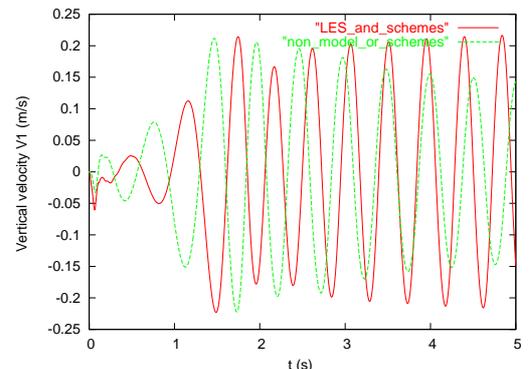

Fig. 5. Effect of Smagorinsky model

Fig. 6. Combined effect

4 Results

4.1 2D Analysis of schemes and model implemented

In this section, the influences of the numerical schemes used and the Smagorinsky approach are presented using two-dimensional grids. In figures 3, 4, 5 and 6 the vertical velocity is

10

plotted at the point 2H from the domain origin (as is showed in figure 1). It can be observed in figure 3 that the use of the Van Leer scheme predicts a different shedding frequency and the signal shows a higher amplitude than the solution without the scheme. An analysis of the results of this simulation permits to confirm that the flow is better predicted using this scheme.

The activation of Adam-Moulton scheme (Fig. 4) initially does not produce significant changes. The amplitude of vertical velocity is practically maintained whereas the non-scheme signal tends to reduce it. Larger differences between signals can be noted after some time of the simulation. Therefore it can be said that a better capture of the instabilities of the flow motion is shown. The Smagorinsky model (fig. 5) induces a cyclic signal earlier than non-model (and scheme) signal but with a smaller amplitude. This behavior gives an idea of the effect of including the turbulent viscosity on the simulation. The differences between signal might be a consequence of modelling, by means of LES model, the energy dissipation from large scales to small scales. The combination of both Van Leer and Adam-Moulton schemes and Smagorinsky model on the simulation (fig. 5) gives a signal with different frequency and amplitude. It can be deduced that this behavior is largely produced by the effects of Smagorinsky model and Van Leer scheme.

4.2 Grid influence

The mean axial velocity over the central plane of domain is shown in figure 7. Four different 2D grids are used. The results of this case show a certain dependency on the grid resolution for the grids used. In figure 7, it is observed that upstream all the runs predict identical results, whereas a faster recovery of mean axial velocity is predicted when the grid resolution is higher but the mean velocity of recirculation is approximately the same in all runs.
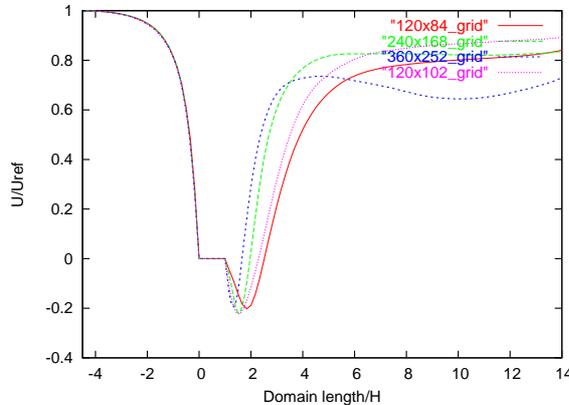

Fig. 7. The mean axial velocity distribution on the center plane of the cylinder from several simulations using different 2D grids

4.3 3D Results

The most important time-averaged parameters of the flow, as defined above, are presented in table 2, where they are also compared with experimental and numerical data available from several authors from the ERCOFTAC database. The labels used are the same as in reference [29]. The parameters compared are the mean drag coefficient, $\overline{C}_D$; its oscillation amplitude, C_D^{rms}; the mean lift coefficient, $\overline{C}_L$, its oscillation amplitude, C_L^{rms}; and the Strouhal number,

Table 2
Comparison among time-averaged square cylinder data. The labels used are the same as in in reference [29]

Reference	Label	$\overline{C}_l$	C_L^{rms}	$\overline{C}_D$	C_D^{rms}	St
Numerical data:						
Verstappen and Veldman [25]	GRO	0.005	1.45	2.09	0.178	0.133
Porquie *et al.* [15]						
-	UK1	-0.02	1.01	2.2	0.14	0.13
-	UK2	-0.04	1.12	2.3	0.14	0.13
-	UK3	-0.05	1.02	2.23	0.13	0.13
Murakami *et al.* [30]	NT	-0.05	1.39	2.05	0.12	0.131
Wang and Vanka [5]	UOI	0.04	1.29	2.03	0.18	0.13
Nozawa and Tamura [12]	TIT	0.0093	1.39	2.62	0.23	0.131
Kawashima and Kawamura [16]						
-	ST2	0.01	1.26	2.72	0.28	0.16
-	ST5	0.009	1.38	2.78	0.28	0.161
Experimental data: Lyn *et al.* [3] [4]	EXP	-	-	2.1	-	0.132
This work	S8A	0.03	1.4	2.01	0.22	0.139

St. It can be noted that the values of this work (label S8A) agree reasonably well with the corresponding experimental and numerical data. The Strouhal number is a slightly greater than experimental data but they have a similar accuracy as the numerical data. The disagreements are due to differences in boundary conditions mainly wall law or damping functions used around the square cylinder.

The mean axial velocity on the center plane of the cylinder is compared in figure 8 with other numerical and experimental values. Labels correspond with the ones shown in table 2. In figure 9, both the experimental data and values from this work are shown. It can be observed from these figures that upstream the data agree very well, whereas after the cylinder the disparity of results is evident. It is important to note that the flow behavior at the inlet is practically laminar and the transition to the turbulence takes places in the shear layers around the square cylinder. This agrees with the experimental work of Lyn and Rody [3]. In figure 9, it can be observed that the results from the simulations of this work agree reasonably well with the experimental data.

An overview of the overall flow pattern can be obtained from the streamlines shown in figure 10. It can be observed that the vortex shedding motion is well captured. This is confirmed in figure 11 where iso-vorticity contours are shown on a (streamwise) $y - z$ plane at $\frac{1}{4}$ and $\frac{3}{4}$ of the vortex shedding period (T). In figure 12, iso-vorticity contours on the (spanwise) $x - z$ plane are shown. Vortical structures over the spanwise direction are weaker than the ones developed over the streamwise direction. However, the three-dimensionality of the simulation is evident.

In figure 13, the turbulent viscosity ν_T around the square cylinder is shown at two times, $\frac{1}{2}$ and $\frac{3}{4}$, of the vortex shedding period (T). It can be observed that ν_T contours are relevant in the areas where the vortex shedding takes place.

The velocity vectors around the square cylinder are shown at four moments of vortex shedding
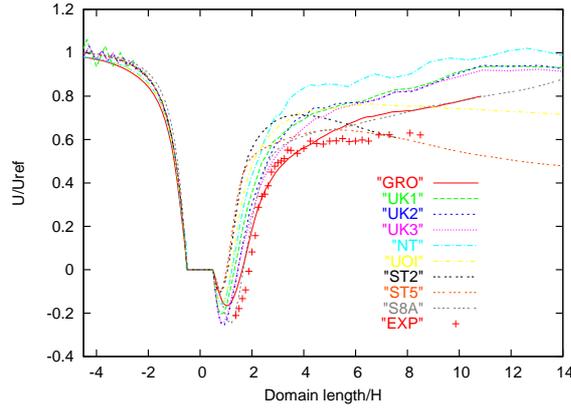
Fig. 8. Comparison among numerical, experimental and this work mean axial velocity on the center plane of the cylinder (labels of table 2)
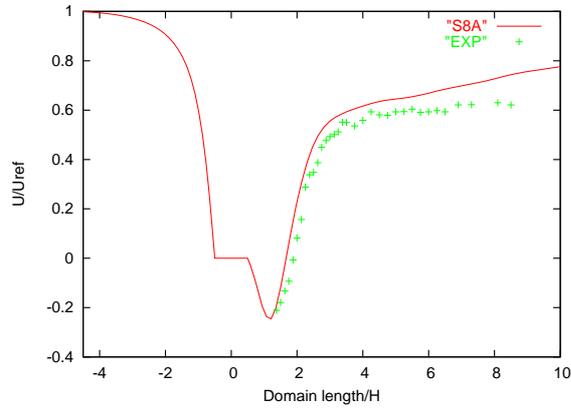

Fig. 9. Comparison between experimental and this work mean axial velocity on the center plane of the cylinder (labels of table 2)
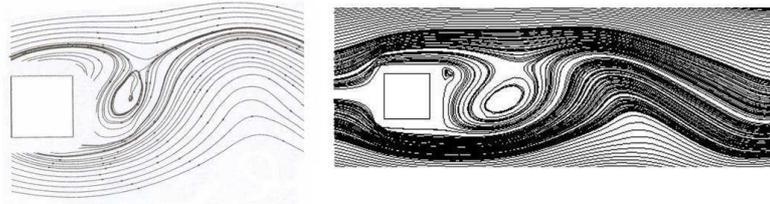

Fig. 10. Experimental and numerical streamlines

cycle in figure 14. The recirculation zone and the vortex shedding are well captured.

4.4 Comparison between LES and RANS simulations

In this section, results obtained from simulations using time-averaged RANS equations with the $k - \epsilon$ model and the implemented LES Smagorinsky model are compared. In $k - \epsilon$ model,
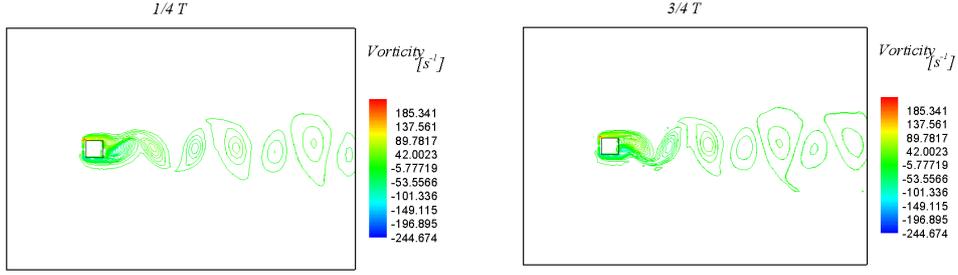
Fig. 11. Iso-vorticity contours of the turbulent flow at two times of the vortex shedding cycle over the streamwise direction ($y - z$ plane, $T = $ vortex shedding period)
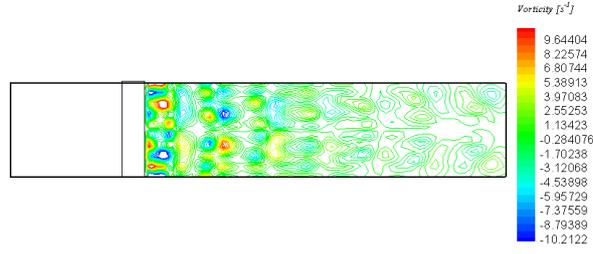

Fig. 12. Iso-vorticity contours of the turbulent flow at two times of the vortex shedding cycle over the spanwise direction ($x - y$ plane, $T = $ vortex shedding period)
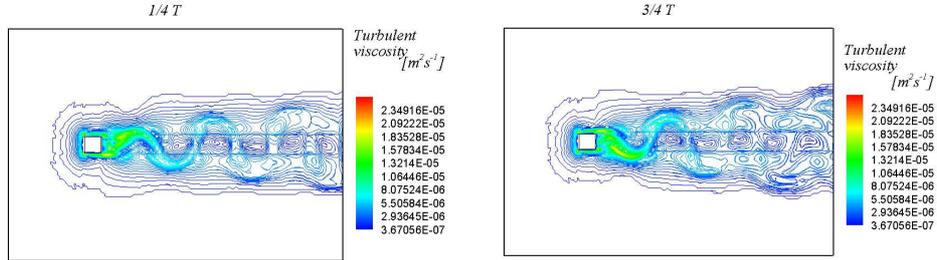

Fig. 13. Turbulent viscosity ν_T around the square cylinder at two times of the vortex shedding cycle ($y - z$ plane, $T = $ vortex shedding period)

ν_t is defined as [10]:

$$\nu_T = C_\mu \frac{k^2}{\epsilon} \qquad (25)$$

where C_μ is a constant ($= 0.09$). Values of k and ϵ are calculated from their respective transport equations.

In figure 15, the vertical velocity is plotted for both $k - \epsilon$ model and LES simulations. Data is obtained in a coordinate point $2H$ from the origin of domain. It can be observed that the
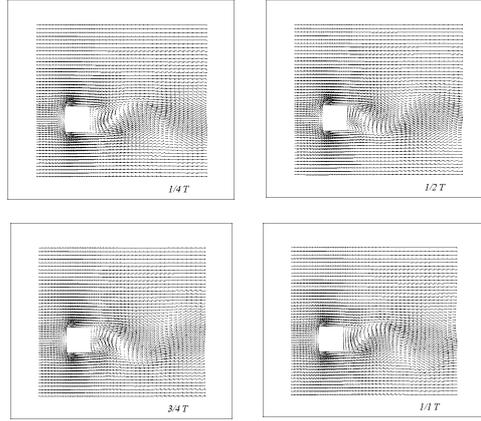
14

Fig. 14. Vector velocity field at four times of the vortex shedding cycle (T = vortex shedding period)

signal amplitude diminishes steadily with the time simulation using $k - \epsilon$ model. This implies that the vortex shedding and flow instabilities tend to disappear in a short time and the flow will become steady. On the contrary, the LES model continues capturing the vortex shedding and flow instabilities.

The mean axial velocity on the center plane of the cylinder is presented in figure 16 for both LES and $k - \epsilon$ model and for the experimental data. It can be observed that $k - \epsilon$ model differs considerably from experimental data. The $k - \epsilon$ model predicts a slow recovery of mean axial velocity after the cylinder.
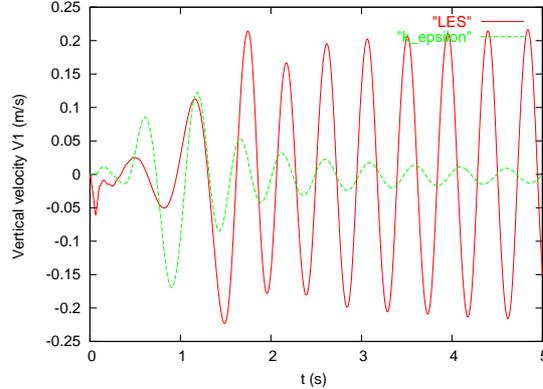

Fig. 15. Comparison between both RANS $k - \epsilon$ model and LES Smagorinsky model of the vertical velocity coordinate point $2H$ from the domain origin

4.5 Parallel performance

The parallel performance of a numerical code is evaluated by the speedup factor which is defined as:
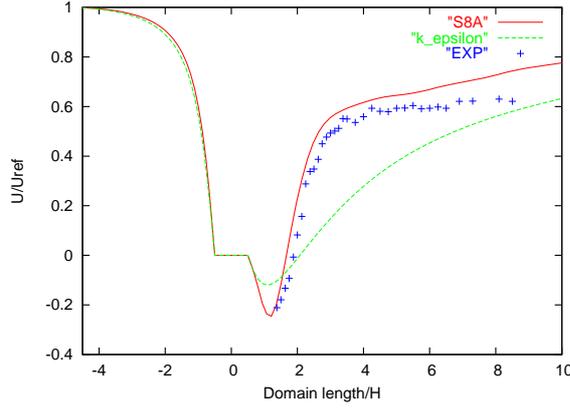
$$S_n = t_1/t_n \tag{26}$$

15

Fig. 16. The mean axial velocity on the center plane of the cylinder using RANS $k - \epsilon$ model and LES Smagorinsky model

where t_1 is the time required to solve a problem using a single processor, t_n is the time required to solve the same problem, but using n processors. Usually, S_n is smaller than n (ideal value) due to communication overheads or load-distribution imbalances. The parallel speedup for this simulation is shown in figure 17. Using a single processor, the calculation required approximately 24 CPU minutes by time step on a 120x102x20 grid. This time can be reduced to approximately 3 minutes per time step when 12 processors are used. Additional processors do not result in a significant speedup for the mesh used.
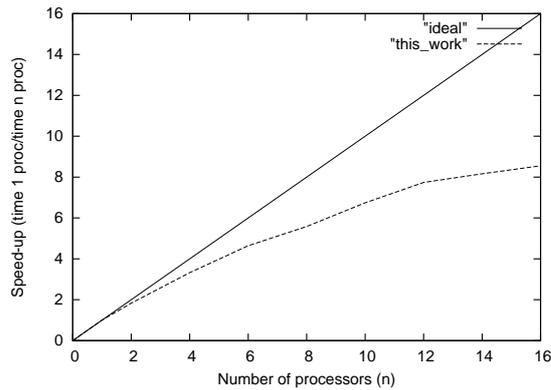

Fig. 17. Parallel performance: speedup as function of number of processors, 120x102x20 grid

5 Conclusions

In this work, a Large Eddy Simulation model has been implemented into PHOENICS and has been applied to simulate the vortex shedding past a square cylinder. The turbulent flow has been simulated using the Smagorinsky subgrid model and high order convective and temporal schemes. The results obtained in this study show a dependency on factors such as the grid resolution, the boundary conditions and the used discretization schemes. It can be concluded from the analysis of simulations that the implementation of LES model and schemes into PHOENICS produces good results with reasonable accuracy.

In this work, it has been also confirmed the superiority (in accuracy) of LES simulations over RANS ones. However, performing LES simulations has a larger computational cost.

Parallelization techniques give a solution that will let in a short time to use this models with more both practical and complex flows.

References

[1]   A. Leonard, Energy cascade in large eddy simulations of turbulent fluid flow. Adv. in Geophys.,18A, p.237. 1974

[2]   D. Bouris and G. Bergeles, 2D LES of vortex shedding from a square cylinder. J. Wind Eng. Ind. Aerodyn., 90 (1999) pp. 31-46.

[3]   D. Lyn and W. Rodi, The flaping shear layer formed by flow separation from the forward corner of a square cylinder. J. Fluid Mech., 267 (1994) pp. 353-376.

[4]   D. Lyn, S. Einav W. Rodi and J. Park, A laser doppler velocimetry study of ensemble-averaged characteristics of the turbulent near wake of a square cylinder. J. Fluid Mech., 304 (1995) pp. 285-319.

[5]   G. Wang and S.P. Vanka, LES of flow over a square cylinder. Department of Mechanical and Industrial Engineering, University of Illinois at Urbana-Champaign, USA, in http://ercoftac.mech.surrey.ac.uk/LESig/les2/

[6]   H. Tennekes and J. L. Lumley, A First Course in Turbulence. MIT Press. 1977

[7]   J. H. Ferziger, Higher Level Simulations of Turbulent Flow, in: Computational Methods for Turbulent, Transonic and Viscous Flows. J. A. Essers ed., Hemisphere. 1983.

[8]   J. H. Ferziger, Large Eddy Simulation, in: Simulation and Modeling of Turbulent Flows. M. Y. Hussaini and T. Gatski, eds., Cambridge University Press. 1996.

[9]   J. H. Peric and M. Ferziger, Computational Methods for Fluid Dynamics. Springer-Verlag Berlin. 1996.

[10]   S. B. Pope, Turbulent Flows. Cambridge University Press. 2003.

[11]   J. Smagorinsky, General Circulation Experiments with the primitive Equations I. The Basic Experiment. Monthly Weather Review 91 (1963). pp. 99-165.

[12]   K. Nozawa and T. Tamura, LES of flow past a squeare cylinder using embedded meshes. Izumi Research Institute and Tokio Institute of Technology, Japan. in http://ercoftac.mech.surrey.ac.uk/LESig/les2/

[13]   M. Breuer and M Pourquié, First Experiences with LES of Flows past Bluff Bodies, in: Proc. of the 3rd Int. Symp. of Eng. Turbulence Modelling and Measurements. Heraklion-Crete, Greece, May 27-29, 1996. Engineering Turbulence Modelling and Experiments 3. W. Rodi and G. Bergeles, eds., Elsevier Science B.V. pp. 177-186.

[14]   M. Breuer and M Pourquié, Large Eddy Simulation of Complex Turbulent Flows of Practical Interest, in: Flow Simulation with High-Performance Computers II. E. H. Hirschel, eds., Notes on Num. Fluid Mech. 52 pp. 258-274, Vieweg Verlag, Braunschweig. 1996.

[15]   M. Porquie, M. Breuer and W. Rodi. Computed test case: square Cylinder. Institute for hydromechanics, University of Karlsruhe, Germany, in http://ercoftac.mech.surrey.ac.uk/LESig/les2/

[16]   N. Kawashima and H. Kawamura, Numerical analysis of flow past a long square cylinder. Department of Mechanical Engineering, Science University of Tokyo, Japan. in http://ercoftac.mech.surrey.ac.uk/LESig/les2/

[17]   N. P. Waterson and Deconinck, A unified Approach to de Design and Application of Bounded Higher-Order Convections Schemes. CFD Lectures Series 1995-21, von Karman Institute for Fluid Dynamics. Rhode-Sain-Genese, Belgium, 1995.

[18]   P. Sagaut, Large Eddy Simulation for Incompressible Flows. Springer-Verlag Berlin Heidelberg 2001.

[19]   P. S. Pacheco, Programming Parallel with MPI. Morgan Kaufmann. San Francisco CA, 1997

[20]   P. S. Pacheco and W. C. Ming, MPI Users' Guide in Fortran. 1997

[21]   P. Voke, Flow past a square Cylinder: Test Case LES2. Department of Mechanical Engineering, University of Surrey, UK. in http://ercoftac.mech.surrey.ac.uk/LESig/les2/

[22]   TR200. The PHOENICS Reference. CHAM, Ltd.

[23]   R. Franke and W. Rodi, Calculation of vortex shedding past a square cylinder with various turbulence models, in: Proc. 8th Symp. Turbulent Shear Flows, 9-11 September 1991. Tech. Univ Munich, Springer Berlin, 1991, pp. 189-204

[24]   R. S. Rogallo and P. Moin, Numerical Simulation of Turbulent Flows. Annual Review of Fluid Mech. 16 (1994) pp.99-137.

[25]   R. Verstappen and A. Veldman, Fourth-Order DNS of flow past a square cylinder: First results. Department of Mathematics, University of Groeningen, The Netherlands, in http://ercoftac.mech.surrey.ac.uk/LESig/les2/

[26]   W. Rodi, On the simulation of turbulent flow past bluff bodies. J. Wind Eng. Ind. Aerodyn., 46-47 (1993) pp. 3-19.

[27]   W. Rodi, Comparisons of LES and RANS calculations of the flow around bluff bodies. J. Wind Eng. Ind. Aerodyn., 69-71 (1997) pp. 55-75.

[28]   W. Rodi, J.H. Ferziger, M. Breuer, and M. Pourquié, in: Proc. Workshop on Large-Eddy Simukation of Flows past Bluff Bodies. Rottach-Egern, Germany, June, 1995.

[29]   W. Rodi, J.H. Ferziger, M. Breuer, and M. Pourquié, Status of large-eddy simulation: Results of a workshop. J. Fluis Eng., 119 (1997) 248-262

[30]   S. Murakami, A. Mochida, On turbulent vortex shedding flow past a square cylinder predicted by CFD. J. Wind Eng. Ind. Aerodyn., 54 (1995) pp. 191-211.

[31]   Schemes for convection discretization. PHOENICS Web Page. http://www.cham.co.uk/phoenics/d_polis/d_enc/enc_schm.htm

[32]   http://ercoftac.mech.surrey.ac.uk/LESig/les2/